Tunnelling and Underground Space Technology 152 (2024) 105906

Contents lists available at ScienceDirect

Tunnelling and Underground Space Technology incorporating Trenchless Technology Research

journal homepage: www.elsevier.com/locate/tust

Real-time forecasting of TBM cutterhead torque and thrust force using aware-context recurrent neural networks

Feng Shan [a], Xuzhen He [a,*], Danial Jahed Armaghani [a], Haoding Xu [a], Xiaoli Liu [b], Daichao Sheng [a]

[a] School of Civil and Environmental Engineering, University of Technology Sydney, NSW, 2007, Australia
[b] State Key Laboratory of Hydroscience and Engineering, Tsinghua University, Beijing, 100084, China

ARTICLE INFO

Keywords:
Tunnel boring machine
Time series forecasting
Cutterhead torque
Thrust force
Recurrent neural network

ABSTRACT

Tunnel Boring Machines (TBMs) are instrumental in the construction of modern tunnels, known for their operational reliability and efficiency. The real-time prediction of cutterhead loads is essential for effective project scheduling, cost management, and risk reduction. This study develops machine learning models for predicting future cutterhead torque and thrust force, simultaneously. The dataset is derived from the Yingsong water diversion project and consists of 12,962 steady-state boring cycles. Because geological conditions and setting values are available in advance, we build a geological parameter-based model and a setting value-based model for regression analysis of cutterhead torque and thrust force. In one-step forecasts, the operational parameter-based model closely captures the trend of the measured results, employing the recurrent neural network (RNN), long short-term memory (LSTM) and gated recurrent unit (GRU). We propose an aware-context recurrent neural network (AC-RNN) model that integrates historical operational parameters and the aware context of setting values, leading to a significant improvement in forecasting accuracy. A sensitivity analysis is carried out to quantify the relative importance of input parameters, revealing that the setting value of revolutions per minute is crucial in forecasting. The results of this study offer valuable practical insights into real-time forecasting, thereby informing engineering applications in this field.

1. Introduction

Mechanised tunnelling, facilitated by Tunnel boring machines (TBMs), is a prevalent methodology in construction projects, including underground mines, subways, railroads, water transportation networks, gas conveyance pipelines, and. TBMs, characterised by the circular full-face cutterhead with disc cutters, are specialised machines for tunnel excavation. TBMs offer many advantages over traditional drilling and blasting, such as increased efficiency, safer working conditions, lower project costs, and minimal disruption to the environment (Rostami, 1997). The process of cutting, mucking, and installing linings is continuously integrated and significantly surpasses the efficiency of traditional methodologies. However, tunnel collapse, rock bursting, water inrush, and machine jamming remain significant impediments, particularly in complicated geological conditions. It is challenging to predict geological conditions with precision before excavation (Qin et al., 2022). The cutterhead load, notably the cutterhead torque (TO) and thrust force (TH), better reflect the change in geological conditions compared with the penetration rate (Zhang et al., 2019). By accurately forecasting the cutterhead torque and thrust force in real time, onsite engineers can promptly adjust TBM operations. This timely intervention substantially enhances both the safety and efficiency of the tunnelling operation.

The cutterhead torque and thrust force, important indicators of TBM performance, are related to various aspects, including machine specifications, geological conditions, and operational parameters. Theoretical methods investigate the mechanics of TBM cutting in the laboratory (Ozdemir, 1977; Rostami et al., 1993; Rostami et al., 1996; Yagiz, 2002) but are limited in correctly representing actual rock mass conditions in the field. Empirical methods study regression equations between TBM performance and field-related parameters (Rostami et al., 1996; Bruland, 1998; Barton, 1999; Yagiz, 2008; Rostami, 2016) but are specific to previous comparable geological conditions. Although the precision of theoretical or empirical methods is acceptable, it is insufficient to meet

* Corresponding author.
E-mail addresses: feng.shan@student.uts.edu.au (F. Shan), xuzhen.he@uts.edu.au (X. He), danial.jahedarmaghani@uts.edu.au (D. Jahed Armaghani), haoding.xu@uts.edu.au (H. Xu), xiaoli.liu@tsinghua.edu.cn (X. Liu), daichao.sheng@uts.edu.au (D. Sheng).

https://doi.org/10.1016/j.tust.2024.105906
Received 12 November 2023; Received in revised form 27 April 2024; Accepted 12 June 2024
Available online 16 June 2024

the need for reliable and efficient construction.

Application of machine learning techniques to TBM tunnelling has proven to be successful in capturing complicated, non-linear relationships, such as surface settlement (Suwansawat et al., 2006; Chen et al., 2019; Zhang et al., 2020), rock mass classification (Sousa et al., 2012; Bo et al., 2022; Hou et al., 2022), and others (Hasanpour et al., 2020; Li et al., 2023). Based on a database of 640 TBM projects in rock, an adaptive neuro-fuzzy inference system (ANIFS) model outperformed several empirical methods for predicting TBM performance (Grima et al., 2000). The ANIFS model was generalised, accounting for geological conditions, operational parameters, and even the type and size of TBMs, but most TBM datasets were not publicly accessible. Using the publicly accessible dataset from the Queen water tunnel with 151 samples, Mahdevari et al. (2014) and Yang et al. (2022) attempted to predict TBM performance using support vector regression (SVR) and random forest (RF), respectively. Interestingly, the sensitivity analysis revealed that the brittleness index was the most sensitive parameter in the RF model (Yang et al., 2022) but the least effective parameter in the SVR model (Mahdevari et al., 2014). The opposite results can be attributed to insufficient training samples, resulting in overfitting or poor generalisation (Shan et al., 2023c). In the project of the Pahang-Selangor raw water transfer tunnel with 1286 samples, machine learning models for predicting TBM performance became more robust and dependable due to increased data and the addition of operational parameters (Armaghani et al., 2017; Koopialipoor et al., 2020; Zhou et al., 2021). However, they are infeasible to apply in practice as operational parameters are unknown inputs during training.

Time series forecasting of TBM performance is a real-time prediction using historical data to predict future TBM performance. It is beneficial to make required changes when potential risks are discovered based on predicted cutterhead torque (TO) and thrust force (TH) ahead of the cutterhead. Moreover, an alarm can be triggered when the predicted TO and TH exceed the maximum values, further safeguarding the tunnelling operation. The data acquisition system collects operational data every few seconds or minutes. One-step forecasts in high frequency can be achieved with high accuracy (Gao et al., 2019; Qin et al., 2021; Shi et al., 2021; Wang et al., 2021a; Qin et al., 2024), but they are less practical to predict TBM performance only a few seconds or centimetres in advance. The accuracy of multi-step forecasts was observed to decrease dramatically as the forecast horizon increased (Shi et al., 2021; Qin et al., 2022). In essential, multi-step forecasts (normally less than ten steps ahead) in high frequency only predict a few seconds or centimetres ahead of the cutterhead. Although such a short time hardly adds any benefit to TBM operators in manual adjustment, high-frequency forecasts can lay the groundwork for future automatic operation systems.

Every data point in low-frequency data is a fixed segment or boring cycle, usually spanning 1–2 m, which is preprocessed by high-frequency data. Xiao et al. (2022) preprocessed data by boring cycle selection, anomaly detection, and noise reduction, resulting in a typical boring cycle with start-up, ascending, steady-state, and end stages. Li et al. (2021), Wang et al., (2021b) and Xu et al. (2021) predicted the average operational parameters at the steady-state stage using the time series from the first two-minute ascending stage. Gao et al. (2020) and Feng et al. (2021) predicted next-step TBM performance using historical data, but training and evaluation are conducted in one project. Shan et al. (2022) successfully built recurrent neural network (RNN) models to predict the next-step penetration rate, 1.5 m ahead, in varying geological conditions, with data from Changsha metro for training and data from Zhengzhou metro for evaluation. However, the model accuracy dramatically decreased when predicting further into the future because of the lower effect further away from the TBM cutterhead (Shan et al., 2022, 2023b).

While forecasting TBM performance has sparked great interest, the question remains: How far ahead can we forecast with acceptable accuracy? On the one hand, high-frequency forecasts are based on historical operational parameters (Gao et al., 2019; Erharter et al., 2021; Qin et al., 2021; Wang et al., 2021a). High-frequency forecasts ignore geological conditions and are not practical in predicting TBM performance a few seconds or centimetres in advance. On the other hand, low-frequency forecasts can predict a few metres ahead, but the data size after preprocessing is limited (Shan et al., 2022), which in turn degrades the robustness of models. Most importantly, reduced accuracy is problematic for multi-step forecasts in low-frequency data.

Given that cutterhead torque and thrust force better capture geological condition changes than penetration rate (Zhang et al., 2019), this study builds robust models to predict these values in the next step, approximately 1.14 m ahead of the cutterhead. We propose an aware-context RNN model to enhance forecasting accuracy by integrating historical operational parameters and aware context of setting values. Additionally, the impact of input parameters is assessed by a sensitivity analysis. Section 2 introduces the Yingsong water diversion project and covers data preprocessing and statistical analysis, and Section 3 presents methodologies of artificial neural network, recurrent neural network, long short-term memory, gated recurrent unit, and aware-context recurrent neural network. A typical modelling process is illustrated in Section 4, detailing the training and testing process. Results for predictions and real-time forecasting are discussed in Sections 5 and Section 6, respectively, highlighting the improved performance of the aware-context recurrent neural network model. Limitations and future research directions are discussed in Section 7, and Section 8 provides a concise summary of the main conclusions

2. Case study

2.1. Project review

The Yingsong water diversion project involved the excavation of a 69.86 km long tunnel to transfer water from the Fengman Reservoir to the city of Changchun and its surrounding areas. The excavation was mainly carried out using TBMs, with supplemental drilling and blasting. In the study, the TBM3 section was excavated using an open-type TBM from July 2015 to February 2018, as specified in Table 1. The TBM excavated a total distance of 17.50 km, with an overburden thickness ranging from 85 to 260 m. The tunnel lithology consists mainly of limestone, diorite, tuff, and granite. Chen et al., (2021b) provided a longitudinal geological profile, detailing the sequence stratigraphy of these rock types.

However, 18 tunnel collapses happened during TBM tunnelling, leading to machine damage, project delays, and increased costs, which are typically attributed to complex rock mass classification. In this project, hydropower classification (HC) is used to categorise surrounding rocks into five classes based on rock solidness and rock mass integrity (Lin, 1999). Quantitatively, an HC index is formulated by evaluating uniaxial compressive strength (UCS) and integrity index K_v, further refined by corrective coefficients of groundwater K_1, structural plane occurrence K_2, and initial in-situ stress K_3, as detailed in Eq. (1) (Wu et al., 2023).

$$\text{HC index} = 100 + 3\text{UCS} + 250K_v - 100(K_1 + K_2 + K_3) \quad (1)$$

Table 1
Main machine parameters of TBM3.

TBM parameters	Value
Weight of TBM	180 (t)
Excavation diameter	7.93 (m)
Number of cutters	56
Maximum thrust force	23,260 (kN)
Cutterhead torque	8410 (kN·m), @ 3.97 rev/min
Revolutions per minute	0–3.97–7.6 (rev/min)

2.2. Data preprocessing

In machine learning, the extraction of condensed and clean feature vectors as inputs and outputs holds significant importance. The acquisition system automatically recorded 199 parameters, archiving them daily in an Excel spreadsheet over a total of 728 days in this study. The chronological and geometrical aspects of the data are characterised by time and chainage, respectively, with time recorded at one-second intervals and chainage measured in metres. The preferred method of data preprocessing hinges on boring cycles, which are categorised into four stages, as delineated in Fig. 1(a).

Start-up stage (S1): the TBM initiates to ramp up. Revolutions per minute (RPM) attain stability, but the TBM does not commence cutting rock.

Ascending stage (S2): the TBM begins to cut rock. Operational parameters of penetration rate (PR), thrust force (TH), and cutterhead torque (TO) increase before achieving dynamic stability.

Steady-state stage (S3): the TBM cuts rock at a constant speed, and four operational parameters remain dynamic stability.

End stage (S4): the TBM gradually halts with four operational parameters decreasing to zero.

TBM operators can adjust the resistance of potentiometers from 0 to 10,000 Ω, regulating the penetration rate (PR_set) and revolutions per minute (RPM_set), as illustrated in Fig. 1(b). PR_set and RPM_set are predetermined prior to the subsequent boring cycle based on sense experience and sparse geological conditions. It is noted that they are displayed values but not intended target values on the control panel. We assume that the setting values align with the target values during the steady-state stage, suggesting that the intended setting values roughly equal the average values during this stage.

However, errors that suddenly exceed one or more orders of magnitude can be caused by machine failure or operator mistakes. An example of such errors is evident in a boring cycle in Fig. 2(a). An error is an unusual data point outside of the data used to build models. Assumed a standard normal distribution, the 3-sigma rule has been extensively used to remove errors (Gao et al., 2020; Feng et al., 2021; Xu et al., 2021), stating that three standard deviations plus or minus the mean encompass 99.73 % of data points. However, errors can distort the mean and standard deviation. We adopted an empirical approach and removed any errors exceeding 200 mm/min. As a result, Fig. 2(b) displays the boring cycle without errors.

This study focuses on TBM performance in the steady-state stage, as it most accurately represents the actual excavation efficiency. This stage entails the bulk of the excavation work and is unaffected by the duration of the boring process. Identifying the turning point between the ascending and steady-state stages, however, poses a challenge. Xu et al. (2021) selected an empirical approximation of the ascending stage at around 2 min. To remove fine vibrations, a moving average technique averages observations over a 20-sliding window to produce a smoothed time series, denoted as PR_20 in Fig. 3. A threshold is then established equal to 0.8 times the median penetration rate. The start and end points are subsequently identified at the intersections between the smoothed time series and the threshold. As a result, we select 12,962 boring cycles of more than 300 data points, i.e., 5 min, during the steady-state stage, averaging a span of 1.14 m. Finally, we computed the average values within the steady-state stage to generate a sample, thus converting high-frequency data into low-frequency data.

2.3. Statistical analysis

Many input parameters are irrelevant to cutterhead torque and thrust force, such as temperature, concentration of O_2, and warning or alarm values. Li et al. (2021) separated them into parameters with constant, low-variance, and highly related values, and the accuracy increased as the input parameters dropped from 154 to 51. PR, RPM, TO, and TH are normally regarded as feature data based on previous knowledge from TBM operation. Several studies only used these four parameters as the input vector (Chen et al., 2021b; Feng et al., 2021; Liu et al., 2021a). Apart from these four parameters, many techniques were employed to find possibly applicable parameters, such as Pearson's correlation (Liu et al., 2021c), variance important measure in the random forest (Li et al., 2021; Guo et al., 2022; Hou et al., 2022). There is no commonly accepted criteria for selecting 199 parameters for the input vector. During TBM construction, TBM operators drive the machine by setting PR_set and RPM_set on the control panel. Fig. 4(a) reveals a strong correlation of 0.832 between PR and PR_set, indicating that the actual penetration rate is influenced by both setting values and geological conditions. Fig. 4(b) demonstrates a linear relationship between RPM and RPM_set, indicating that the setting values of revolutions are promptly reflected in the actual revolutions.

Regarding geological conditions, hydropower classification (HC) and fault zone (FZ) are measured during site investigation. Geological data is

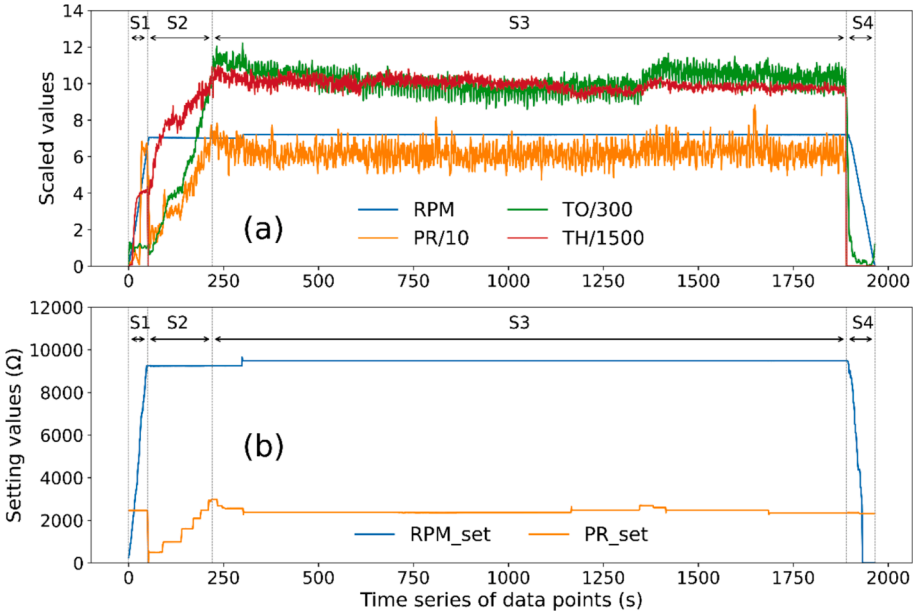

Fig. 1. Typical boring cycle in (a) operational parameters and (b) setting values.

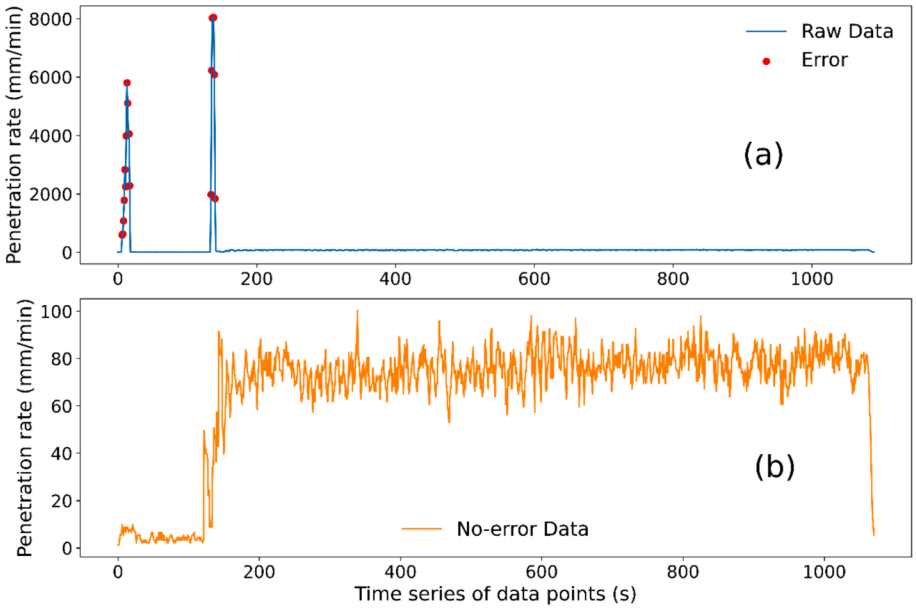

Fig. 2. Specific boring cycle (a) with errors and (b) removing errors.

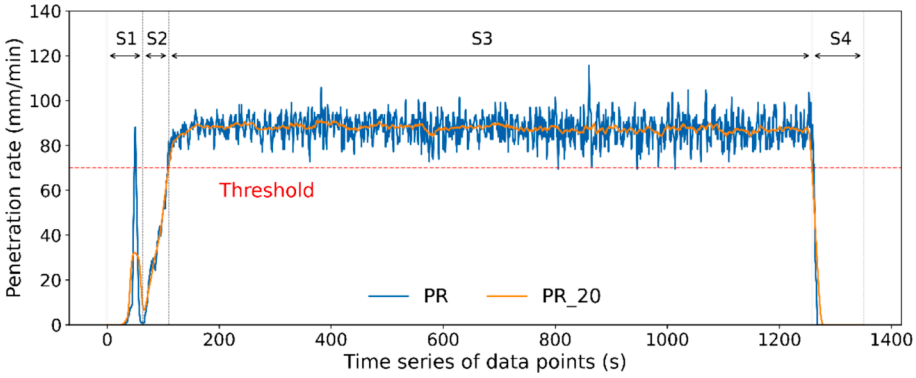

Fig. 3. Segmentation for steady-state boring cycles via moving average and threshold method.

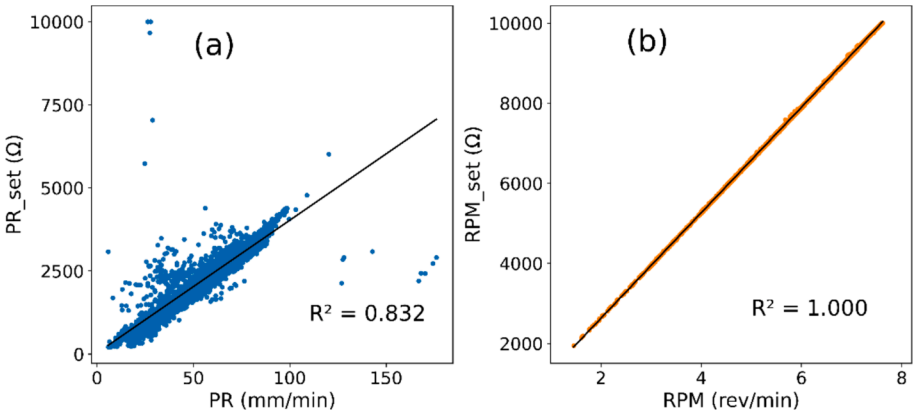

Fig. 4. Scatter plots and correlations for (a) PR versus PR_set, and (b) RPM versus RPM_set.

approximately fitted according to the chainage along the tunnel alignment to balance the sampling of operational data. While the wear condition of individual cutters significantly affects thrust and torque, TBM operators replaced cutters at varying frequencies depending on their wear conditions at different positions. For example, during a 17.5 km excavation, cutter No. 9 was replaced 6 times, while cutter No. 51 was replaced 93 times. Therefore, we ignored wear conditions of cutters and assumed that all 56 cutters on the cutterhead maintain a relatively constant state of wear. Please note that we theoretically could not consider a constant value as one of the inputs in machine learning models since it has a very limited influence on the model output.

In this study, the input vector consists of four operational parameters

(PR, RPM, TO, and TH), two geological parameters (HC and FZ), and two setting values (PR_set and RPM_set). The output vectors are TO and TH in the next step. Statistical details of these parameters are summarised in Table 2.

3. Machine learning algorithm

3.1. Artificial neural network

The artificial neural network (ANN) can imitate the response of the biological nervous system to external stimuli (Jain et al., 1996). The components of ANN include an input layer, one or more hidden layers, and an output layer, which are fully connected between layers expressed as Eqs. (1)–(2).

$$h = \mathrm{ReLU}(Ux + b_h) \tag{1}$$

$$y = Vh + b_o \tag{2}$$

where x ,h and y represent input, hidden, and output nodes, respectively; U and b_h are unknown weight and bias in the hidden layer; V and b_o are unknown weight and bias in the output layer. ReLU(x), an activation function, behaves as a linear function when x is greater than 0 and becomes 0 otherwise. Notably, no activation function is applied in the last hidden layer of Eq. (2), also known as a fully connected layer with extracted features. Overfitting is a main issue in ANN, often resulting from excessive feature dimensions, overly complex structures, an abundance of noise, or insufficient training data (Srivastava et al., 2014).

3.2. Recurrent neural network

The recurrent neural network (RNN) is a popular algorithm for speech recognition, language translation, and time series forecasting because of its internal state (Schuster et al., 1997). Fig. 5 shows how information is transferred from earlier neurons to later neurons in the RNN model. In Eq. (3), the recent hidden state h_t is influenced by the recent inputs x_t and last hidden state h_{t-1}. The recent output y_t applies a linear transformation in Eq. (4) to extract temporal information from the recent hidden state.

$$h_t = \tanh(Ux_t + Vh_{t-1} + b_h) \tag{3}$$

$$y_t = Wh_t + b_o \tag{4}$$

where U and V are weights in the hidden layer; W are weights in the output layer. tanh(x) is an activation function that yields the hyperbolic tangent of the input. Long-term dependencies in time series are challenging for RNN to capture because of vanishing or exploding gradients (Hochreiter, 1998).

Table 2
Basic statistical details of parameters.

Parameters	Abbreviation	Unit	Min.	Max.	Ave.
Penetration rate	PR	mm/min	5.80	176.08	62.95
Revolutions per minute	RPM	rev/min	1.456	7.621	6.287
Cutterhead torque	TO	kN·m	118	3876	2288
Thrust force	TH	kN	2763	19,810	12,406
Hydropower classification	HC	–	2	5	3.32
Fault zone	FZ	–	0	1	0.010
Setting value of penetration rate	PR_set	Ω	212	10,000	2547
Setting value of revolutions per minute	RPM_set	Ω	1944	10,000	8278

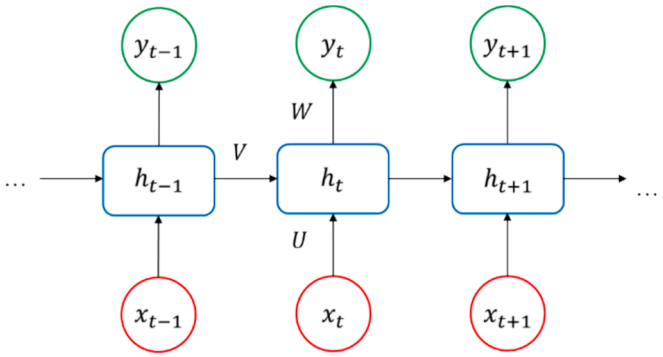

Fig. 5. Structural diagram of a RNN model.

3.3. Long short-term memory

The long short-term memory (LSTM), a particular kind of RNN, is designed to capture long-term dependencies and to address the issue of vanishing or exploding gradients (Hochreiter et al., 1997). An LSTM memory cell has the forget gate f_t, input gate i_t, output gate o_t, and input node $\tilde{c}_t$, as shown in Fig. 6. The gates allow it to discard irrelevant information and preserve relevant information, resulting in the cell state c_t and hidden state h_t being updated over time, which are expressed as Eqs. (5)–(10).

$$f_t = \sigma\left(U_f x_t + V_f h_{t-1} + b_f\right) \tag{5}$$

$$i_t = \sigma(U_i x_t + V_i h_{t-1} + b_i) \tag{6}$$

$$o_t = \sigma(U_o x_t + V_o h_{t-1} + b_o) \tag{7}$$

$$\tilde{c}_t = \tanh(U_c x_t + V_c h_{t-1} + b_c) \tag{8}$$

$$c_t = f_t \circ c_{t-1} + i_t \circ \tilde{c}_t \tag{9}$$

$$h_t = \tanh(c_t) \circ o_t \tag{10}$$

where subscripts f, i, o, c represent the forget gate, input gate, output gate, and input node; the operator $\circ$ is the element-wise product in mathematics; $\sigma(x)$ is a sigmoid activation function applied to learn complex patterns in the data, with return value commonly monotonically increasing.

3.4. Gated recurrent unit

The gated recurrent unit (GRU) is a more simple form of LSTM, handling inputs of varying lengths and capturing temporal dependencies (Cho et al., 2014). Its less complex structure allows for quicker training

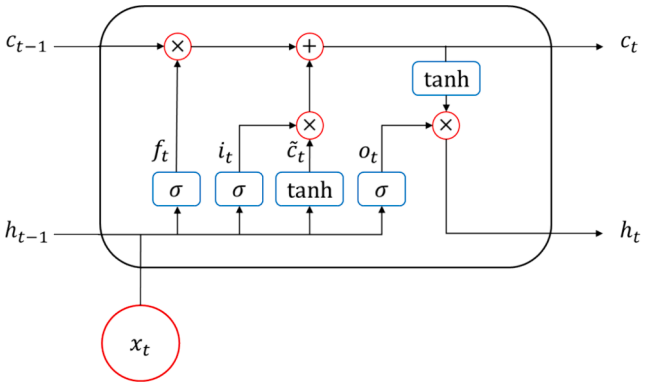

Fig. 6. Structural diagram of an LSTM memory cell.

times and reduced computational demands due to fewer parameters. The key innovation of GRU lies in the reset gate r_t and update gate z_t, which control the flow of information in Fig. 7. These gates are learned automatically in Eqs. (11–12), facilitating the candidate hidden state $\widetilde{h}_t$ and hidden state h_t in Eqs. (13)–(14), without running into issues of vanishing or exploding gradients.

$$r_t = \sigma(U_r x_t + V_r h_{t-1} + b_r) \tag{11}$$

$$z_t = \sigma(U_z x_t + V_z h_{t-1} + b_z) \tag{12}$$

$$\widetilde{h}_t = \tanh(U_h x_t + V_h(r_t \circ h_{t-1}) + b_h) \tag{13}$$

$$h_t = z_t \circ h_{t-1} + (1 - z_t) \circ \widetilde{h}_t \tag{14}$$

where subscripts r, z, h represent the reset gate, update gate, and candidate hidden state.

3.5. Aware-context recurrent neural network

There are other parameters than the sequential data that affect future values but are not time-dependent, so data inputs can be categorised as either sequential or non-sequential. Due to their loop architecture, RNN, LSTM and GRU can handle sequential data well but not non-sequential data. We develop an aware-context recurrent neural network (AC-RNN) model combined with sequential operational parameters and non-sequential setting values.

In Fig. 8, the hidden layer of RNN processes sequential data x_{t-2}, x_{t-1} and x_t in Eq. (3), generating the recent hidden state h_t. Non-sequential data $\bar{x}_t$ are fully connected to extract hidden features $\bar{h}_t$ in Eq. (1). A fully connected layer then concatenates the recent hidden state and hidden features. The final output layer y_{t+1} is fully connected in Eq. (4) (Shan et al., 2023a). The AC-RNN model utilises a combination of sequential and non-sequential data, deeply mining the available information for time series forecasting.

4. Modelling process

The flowchart on the left side of Fig. 9 outlines the steps in the modelling process. The data are detailed on the right side of Fig. 9, including operational and geological data, as well as the aware context of setting values, all presented in a low-frequency format. To address the issue of varying units and magnitudes among parameters, the min–max normalisation is applied, scaling data between 0 and 1. This normalisation stabilises gradient descent and facilitates faster convergence of the model. It is worth noting that the outputs are scaled back to the original scale after performing the model.

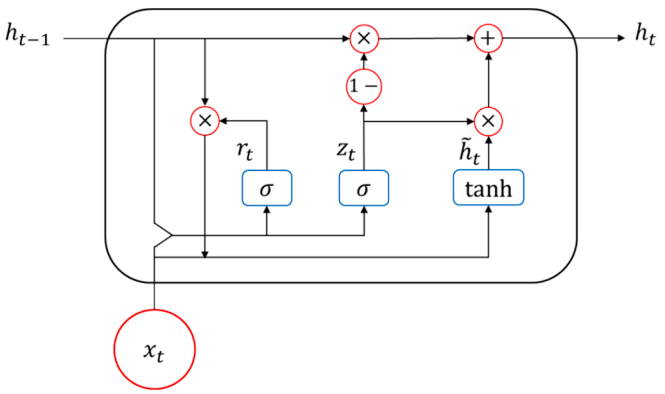

Fig. 7. Structural diagram of a GRU memory cell.

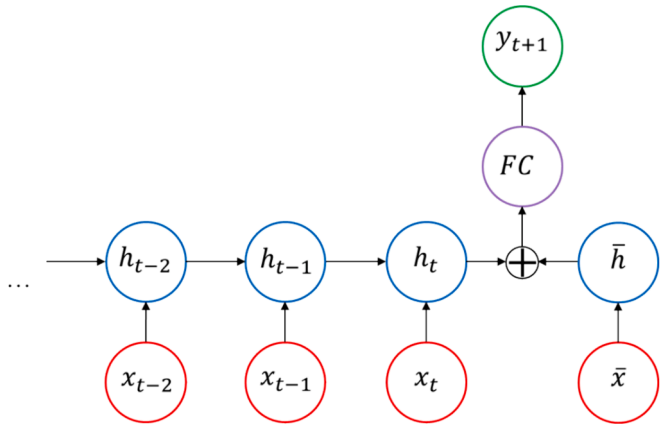

Fig. 8. Structural diagram of an AC-RNN model.

4.1. Training

In the training process, several machine learning models are applied to build a model in the 60 % training data, using the Adam optimiser and the mean squared error (MSE) loss function in Eq. (15). The training process involves 50 epochs to iteratively update weights and biases. In order to avoid overfitting, a dropout rate is implemented as a regularisation technique that randomly sets a portion of input nodes to zero during training (Srivastava et al., 2014).

$$\text{MSE} = \frac{1}{n}\sum_{i=1}^{n}(y_i - \hat{y}_i)^2 \tag{15}$$

A separate validation dataset of 20 % is used to tune hyperparameters not trained in the training process. These hyperparameters include time step [1, 2, 3, 5, 7, 10], number of layers [1, 2, 3], hidden size [8, 16, 32, 64, 128], learning rate [0.001, 0.01], dropout rate [0, 0.2, 0.5], and batch size [32, 64, 128]. Grid search exhaustively searches the predefined search space to find the best combination of hyperparameters, running 1620 trials (=6 × 3 × 2 × 5 × 3 × 3). Alternatively, random search is computationally efficient and focuses on randomly sampling different combinations. In this study, 60 random trials are conducted, providing a 95 % probability of finding a combination within the top 5 % of optima (Bergstra et al., 2012).

4.2. Evaluation

A near-optimal model is trained and evaluated using 20 % test data, assessing the model performance and generalisation ability. The near-optimal model is evaluated by the mean absolute percentage error (MAPE) and coefficient of determination (R^2), as presented in Eqs. (16)–(17).

$$\text{MAPE} = \frac{1}{n}\sum_{i=1}^{n}\left|\frac{y_i - \hat{y}_i}{y_i}\right| \tag{16}$$

$$\text{R}^2 = 1 - \frac{\sum_{i=1}^{n}(y_i - \hat{y}_i)^2}{\sum_{i=1}^{n}(y_i - \bar{y})^2} \tag{17}$$

where $y, \hat{y}$ are measured and predicted values, and $\bar{y}$ is the average of the measured values. MAPE is non-dimensional and evaluates prediction error in percentage. R^2 is a performance indicator ranging from 0 to 1, with a larger value indicating higher accuracy between predicted and measured values, and vice versa.

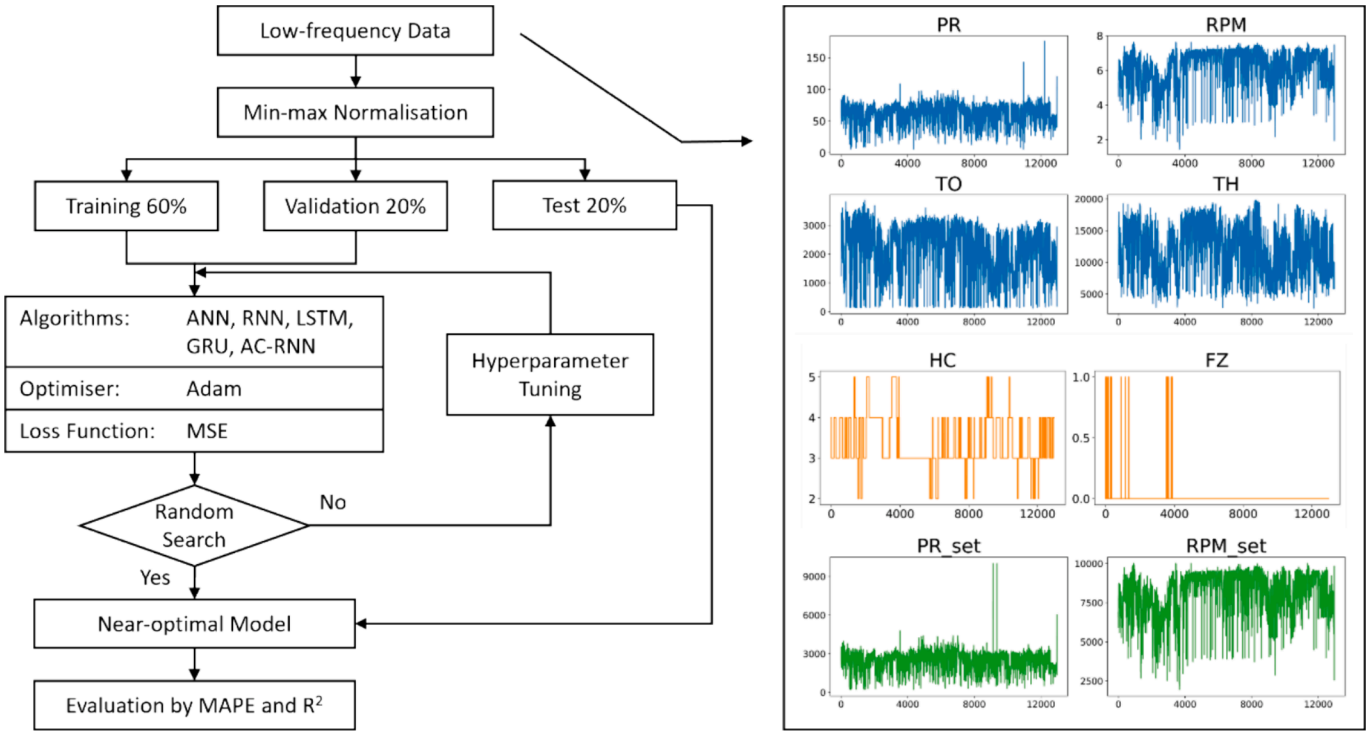

Fig. 9. Flowchart of the modelling process and low-frequency data.

5. Predicting cutterhead torque and thrust force

5.1. Geological parameter-based model

During the training process, operational parameters of PR, RPM, TO, and TH are inaccessible. The model based on operational parameters is impractical for real-world applications, even having high accuracy. Since geological conditions are measured via site investigation and available before tunnelling, we apply a model based on geological parameters before the start of the project, expressed as Eq. (18).

$$\mathrm{TO},\ \mathrm{TH} = f(\mathrm{HC}, \mathrm{FZ}) \tag{18}$$

where geological parameters of HC and FZ are the input vector, and TO and TH are the output vector. The weight matrix and bias are training arguments in the machine learning algorithm $f(x)$, which employs ANN here.

Fig. 10 illustrates the testing performance of the near-optimal model, with MAPE of 0.401 and R^2 of 0.337 for cutterhead torque, and MAPE of 0.258 and R^2 of 0.290 for thrust force. Given that geological conditions are sparsely sampled with localised information, the predicted results appear stepwise. Therefore, these geological conditions fail to capture the temporal changes in TBM performance.

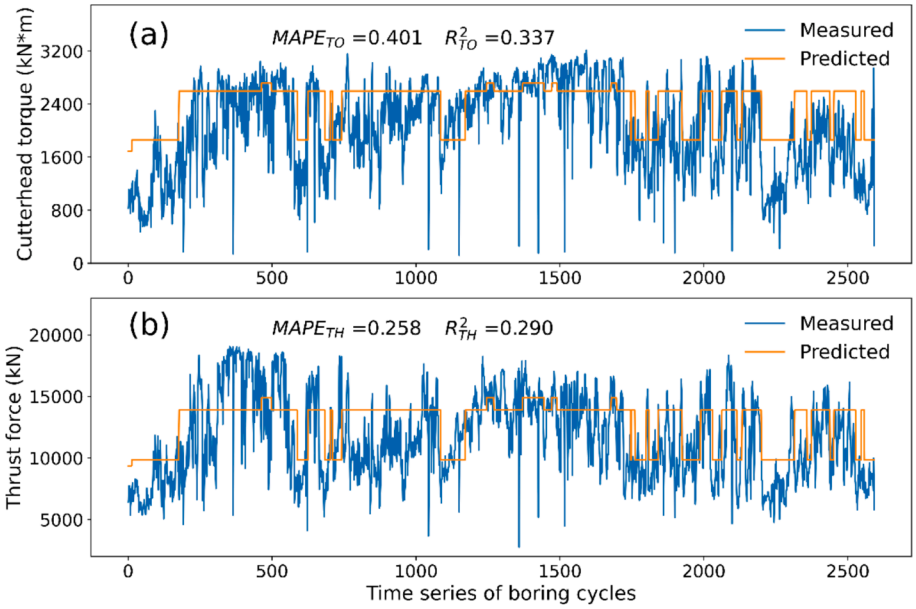

Fig. 10. Measured and predicted results for predicting (a) cutterhead torque and (b) thrust force in the geological parameter-based model.

5.2. Setting value-based model

Before proceeding to the next boring cycle, PR_set and RPM_set are predetermined, taking into account operators' experience and limited geological conditions. When predicting the next-step cutterhead torque and thrust force, the setting values for the next step are already known in advance. When it comes to multi-step forecasts, PR_set and RPM_set are not accessible because they are too far away from the cutterhead. The setting values, while effective for one-step forecasts, are not as well-suited for multi-step forecasts. The model based on setting values is represented by Eq. (19)

$$\mathrm{TO}_{t+1}, \mathrm{TH}_{t+1} = f(\mathrm{PR\_set}_{t+1}, \mathrm{RPM\_set}_{t+1}) \tag{19}$$

where PR_set $_{t+1}$ and RPM_set $_{t+1}$ are the setting values for the upcoming cycle and form the input vector. The cutterhead torque and thrust force in the next cycles, TO $_{t+1}$ and TH $_{t+1}$, are the output vector. The machine learning algorithm used in this case is ANN.

Fig. 11(a) and 11(b) illustrate that the predicted results generally align with the trend of measured results during testing, characterised by MAPE of 0.335 and R^2 of 0.654, and MAPE of 0.193 and R^2 of 0.702, respectively. This degree of alignment suggests that PR_set and RPM_set indeed have an influence on the performance of both cutterhead torque and thrust force.

6. Time series forecasting

6.1. Operational parameter-based model

One-step forecasts in low frequency are to simultaneously predict the cutterhead torque and thrust force in the next boring cycle, around 1.14 m ahead of the cutterhead. Time series forecasting uses historical operational parameters as the input vector to predict the next-step TBM performance in Eq. (20). A random search process determines the combination of hyperparameters that yields a near-optimal RNN model. These hyperparameters include a time step of 7, a number of layers of 3, a learning rate of 0.001, a hidden size of 32, a dropout rate of 0, and a batch size of 32.

$$\mathrm{TO}_{t+1}, \mathrm{TH}_{t+1} = f(\{\mathrm{PR}_t, \mathrm{RPM}_t, \mathrm{TO}_t, \mathrm{TH}_t\}) \tag{20}$$

The trained RNN model is then assessed using unseen test data, constituting 20 % of the dataset, as depicted in Fig. 12. It is observed that the predicted results in orange demonstrate a close alignment with the measured results in blue, with MAPE of 0.168 and R^2 of 0.773 for cutterhead torque, and MAPE of 0.093 and R^2 of 0.820 for thrust force.

Apart from TO, TH, PR, and RPM, we built an operational parameter-based model with 16 inputs. These include face pressure, left shield pressure, right shield pressure, top shield pressure, gripper pressure, left support pressure, right support pressure, cutterhead jetting pressure, pitch angle of front shield, rolling angle of front shield, cutterhead power, and screw conveyor rotational speed.

The measured and predicted results are shown in Fig. 13 and are compared against the 4-input model in Table 3. However, it may seem to be counter-intuitive that the 16-input RNN model performs a bit worse than the 4-input RNN model in this study. It is because while these parameters are related to TO and TH in the regression model, the focus here is on time series forecasting to predict future TO and TH. The statement is supported by sensitivity analysis in Section 6.4, which indicates that historical parameters (except TO or TH) have little influence on the next step of TO or TH.

6.2. Comparison between machine learning algorithms

LSTM and GRU are two popular variants of RNNs designed to address the vanishing or exploding gradients, allowing them to capture long-term dependencies more effectively. To compare these with the RNN model, LSTM and GRU models are built for one-step forecasts. In Table 4, MAPEs for cutterhead torque are 0.168, 0.170, and 0.167, and corresponding R^2 of 0.773, 0.770, and 0.773 in the RNN, LSTM, and GRU models, respectively. MAPEs for thrust force are 0.093, 0.091, and 0.093, and corresponding R^2 of 0.820, 0.820, and 0.821 in the RNN, LSTM, and GRU models, respectively. These results reveal negligible differences among these algorithms, suggesting that long-term information has limited influence on future TBM performance, supported by sensitivity analysis in Section 6.4. This implies that the time series of TBM performance behaves like a random walk (Shan et al., 2022), lacking long-term trends and periodicity.

6.3. Setting value and operational parameter-based model

PR_set and RPM_set are manually set on the control panel, directly influencing the actual penetration rate and revolutions in TBM tunnel-

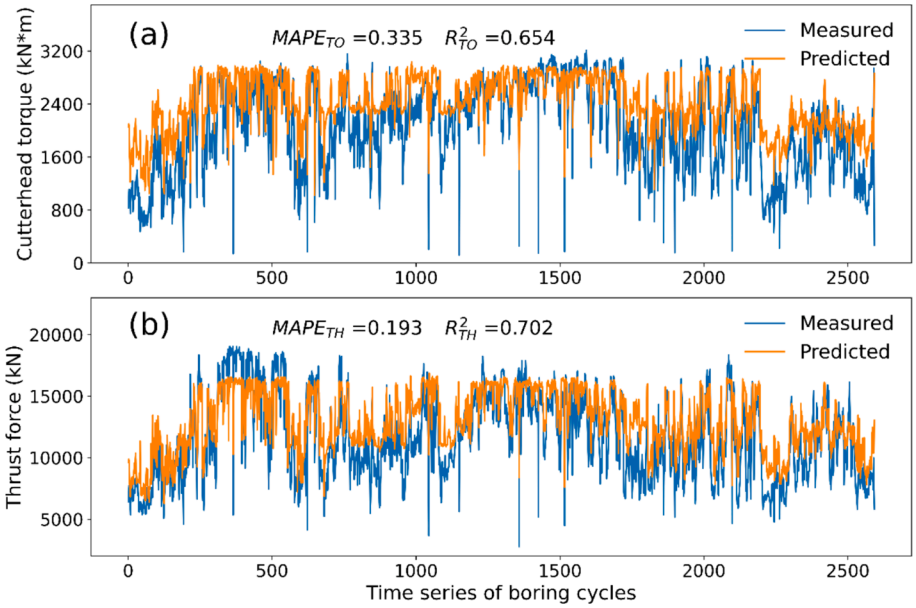

Fig. 11. Measured and predicted results for predicting (a) cutterhead torque and (b) thrust force in the setting value-based model.

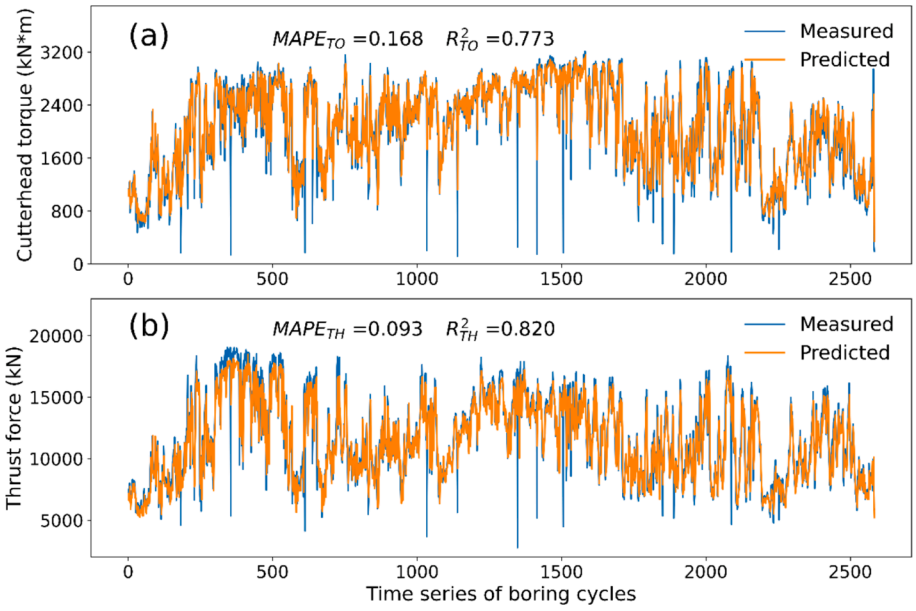

Fig. 12. Measured and predicted results for time series forecasting of (a) cutterhead torque and (b) thrust force using 4 operational inputs.

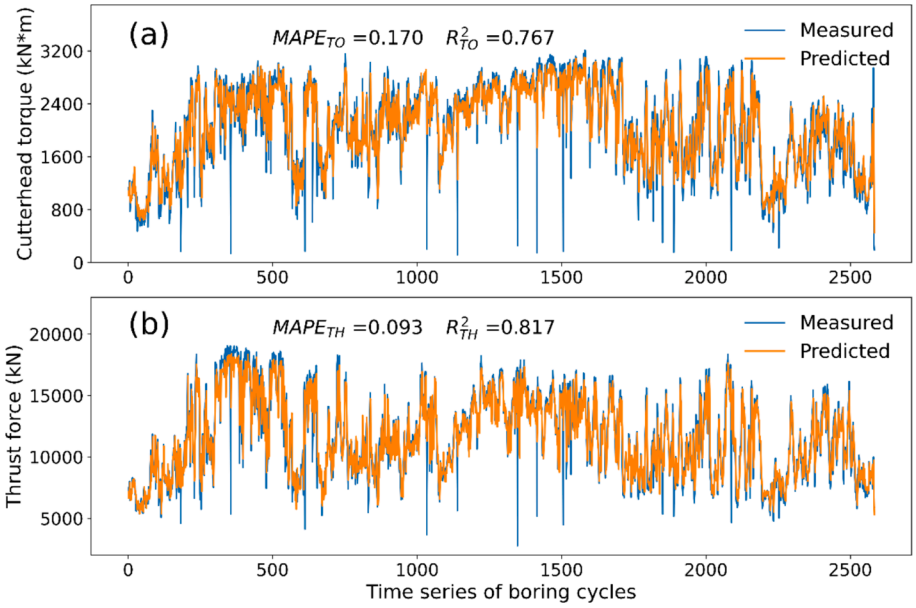

Fig. 13. Measured and predicted results for time series forecasting of (a) cutterhead torque and (b) thrust force using 16 operational inputs.

Table 3
Comparison of 4-input and 16-input models.

Algorithm	Input	TO		TH	
		MAPE	R^2	MAPE	R^2
RNN	4 operational inputs	0.168	0.773	0.093	0.820
RNN	16 operational inputs	0.170	0.767	0.093	0.817

Table 4
Comparison of RNN, LSTM, and GRU models.

Algorithm	Input	TO		TH	
		MAPE	R^2	MAPE	R^2
RNN	4 operational inputs	0.168	0.773	0.093	0.820
LSTM	4 operational inputs	0.170	0.770	0.091	0.820
GRU	4 operational inputs	0.167	0.773	0.093	0.821

ling. When predicting the next-step TBM performance, the setting values for the next step are already known beforehand. As setting values are the aware context, the proposed model is referred to as the AC-RNN model in Eq. (21).

$$\mathrm{TO}_{t+1}, \mathrm{TH}_{t+1} = f(\{\mathrm{PR}_t, \mathrm{RPM}_t, \mathrm{TO}_t, \mathrm{TH}_t\}, \mathrm{PR\_set}_{t+1}, \mathrm{RPM\_set}_{t+1}) \quad (21)$$

In the training process, inputs are reconfigured into two components: sequential inputs of historical operational data and non-sequential inputs of setting values. The historical data (PR, RPM, TO, and TH) are fed into the RNN hidden layer, producing recent hidden state. At the same time, the setting values (PR_set and RPM_set) are fully connected to extract hidden features. These hidden features are concatenated in a fully connected layer, ultimately producing the next-step cutterhead

torque and thrust force. Notably, the hidden layer within RNN can also be substituted with LSTM or GRU memory cells. However, the difference amongst these algorithms is marginal for forecasting TBM performance in Section 6.2, so we focus on the AC-RNN model in this study.

The optimal combination of hyperparameters for the AC-RNN model includes a time step of 7, a number of layers of 2, a learning rate of 0.001, a hidden size of 32 for historical operational parameters, a hidden size of 32 for setting values, a dropout rate of 0, and a batch size of 32. In Fig. 14, measured and predicted results are illustrated, having improved MAPE of 0.15 and R^2 of 0.808 for cutterhead torque, and improved MAPE of 0.088 and R^2 of 0.852 for thrust force.

Fig. 15 shows testing performance for one-step forecasts employing the geological parameter-based, setting value-based, operational parameter-based, and setting value and operational parameter-based models. In comparisons, the setting value and operational parameter-based model, or AC-RNN model, demonstrates superior performance, with a reduction in MAPE from 0.401, 0.335, and 0.168 to 0.150 for cutterhead toque, and a reduction in MAPE from 0.258, 0.193, and 0.093 to 0.088 for thrust force in Fig. 15(a). Model performance measured by R^2 is compared on input parameters in Fig. 15(b). For cutterhead torque forecasts, the model incorporating setting value and operational parameters achieves R^2 of 0.808, which is significantly higher than other models. This model also attains the highest R^2 of 0.852 for thrust force forecasts.

In general, the accuracy of thrust force forecasts is higher than that of cutterhead torque forecasts in the models. This discrepancy can be explained by the fact that the cutterhead torque time series exhibits more rapid changes than the thrust force. These rapidly changing points, or minimal features, can often be overlooked by machine learning models, leading to less accurate predictions.

6.4. Sensitivity analysis

From a quantitative perspective, the Sobol method is employed to analyse the sensitivity of the input parameters and observe their variations in model output (Sobol, 1990). The near-optimal AC-RNN model accounts for four operational parameters of the last seven steps and the two setting values for the next step. We investigate the importance of the input parameters, where the total Sobol index equals the sum of the Sobol indexes across the last seven steps. When forecasting cutterhead torque on the left side of Fig. 16, RPM_set is the most important parameter with a Sobol index of 0.468, while historical revolution $\{RPM_t\}$ contributes merely 0.056 to the index. Historical cutterhead torque $\{TO_t\}$ is the second-order sensitive parameter with a Sobol index of 0.242. For forecasting thrust force on the right side of Fig. 16, historical thrust force $\{TH_t\}$ itself exerts a significant influence on the next-step thrust force with a Sobol index of 0.468, followed by RPM_set with an index of 0.354. It is found that TBM performance in the next step is greatly related to the setting values, especially RPM_set.

To analyse the effect of time steps, the heatmaps of the Sobol index for cutterhead torque and thrust force are presented in Fig. 17(a) and 17 (b), respectively. The Sobol indexes from the last seven steps to three steps fall below 0.01, suggesting their minimal influence on future TBM performance. This indicates that operational parameters further away from the current cutterhead have negligible effects, thus explaining why LSTM and GRU, which are capable of long-term dependencies, perform equivalently to RNN. The Sobol index of the last-step operational parameters outperforms that of other time steps. In detail, for forecasting cutterhead torque, the last-step cutterhead torque TO_t has the highest Sobol index of 0.23, while for forecasting thrust force, the last-step thrust force TH_t scores the highest Sobol index of 0.44.

7. Limitations and future studies

The lack of interpretability in machine learning models, known as the black box problem, is a primary disadvantage. While these models excel at capturing complex patterns and relationships in data for making predictions, understanding the rationale behind their decisions can be challenging. To address this limitation, this study assesses the influence of input variables on the output by Sobol index, providing insights into feature selection in machine learning. Promising methods for TBM tunnelling include theory-guided machine learning (Karpatne et al., 2017) and physics-informed neural networks (Chen et al., 2021a) in future studies. The methods enable the ability to find the best solutions and generalise effectively by incorporating prior knowledge of theory or physical laws into the training process.

Another crucial restriction lies in the limited applicability of models developed and validated on a single dataset. To gain confidence for the industry, it is necessary to validate and generalise these models across diverse datasets. As tunnelling data becomes more accessible, expanding

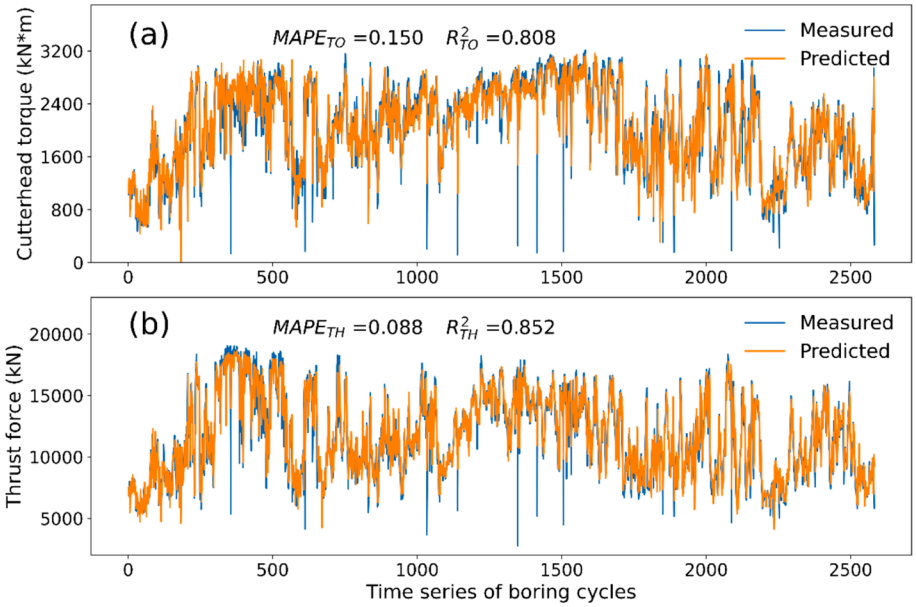

Fig. 14. Measured and predicted results for time series forecasting of (a) cutterhead torque and (b) thrust force in the setting value and operational parameter-based model.

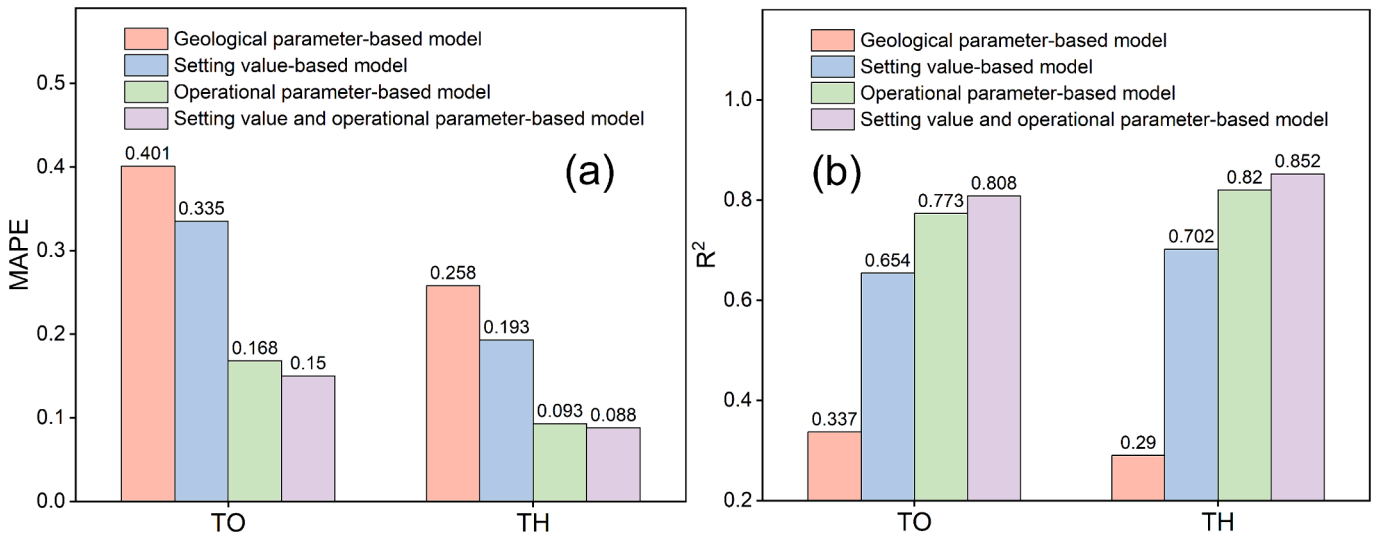

Fig. 15. Comparison of input parameters in terms of (a) MAPE and (b) $R^{2.}$

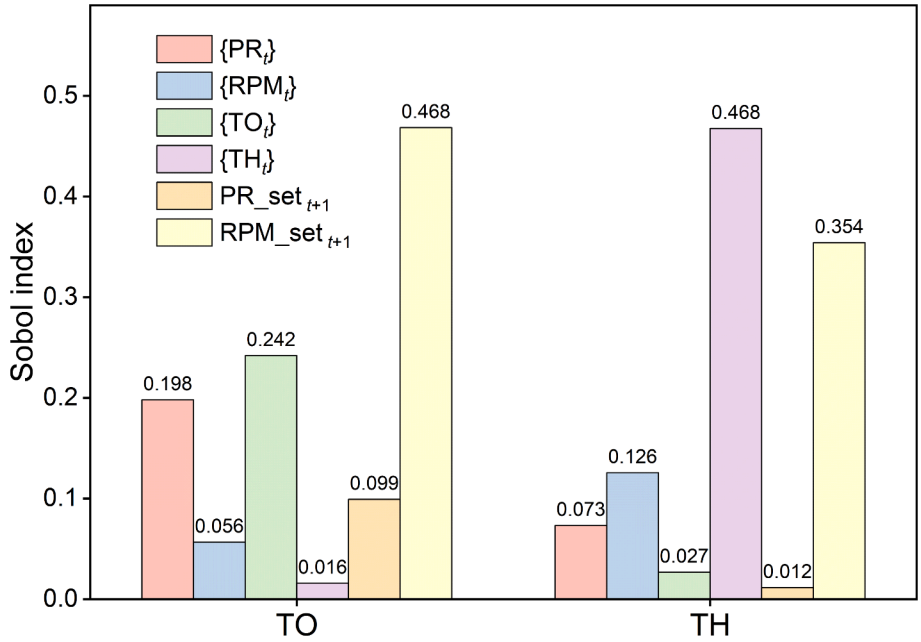

Fig. 16. Cumulative Sobol index of input parameters.

the training data can further improve the dependability and robustness of machine learning models in future endeavours, providing valuable insights into the industry.

This study focuses on one-step forecasts of cutterhead torque and thrust force, around 1.14 m ahead of the cutterhead. However, the multi-step forecasts in low frequency become novel and challenging: the accuracy tends to diminish with an increasing forecast horizon (Shan et al., 2022). Regarding input parameters in this study, historical operational parameters become less related to further TBM performance; setting values for multi-step forecasts are inherently uncertain, as they are too far away to know; the geological conditions from site investigations are known before the start of a project but offer only a rough estimation and lack precise reliability. Apart from operational data, vibration data on the cutterhead are promising to reflect geological conditions in the future, such as soil-rock interfaces (Liu et al., 2021b; Shen et al., 2023).

8. Conclusion

This study utilises machine learning techniques to predict the next-step cutterhead torque and thrust force, simultaneously. The dataset, derived from the Yingsong water diversion project, is preprocessed into low-frequency data so that every sample represents the average of a steady-state boring cycle. The input vector in the modelling process encompasses operational parameters of PR, RPM, TH, and TO, geological parameters of HC and FZ, and setting values of PR_set and RPM_set.

The geological parameter-based model fails to regress TBM performance as HC and FZ are approximating from sparse sampling. Considering PR_set and RPM_set are predetermined, we build the setting value-based model to regress TO and TH that align with the general trends. It shows that setting values have an influence on the performance of both cutterhead torque and thrust force.

Time series forecasting using historical operational parameters is explored in terms of input parameters and algorithms. The 16-input

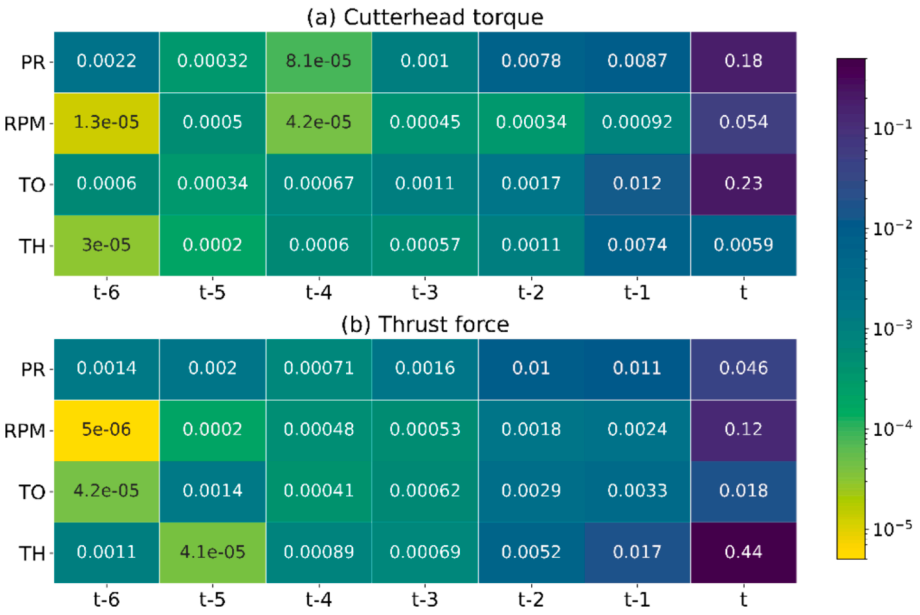

Fig. 17. Temporal Sobol index of input parameters: (a) cutterhead torque and (b) thrust force.

model performs slightly worse than the 4-input model, as historical parameters (except TO or TH) have little influence on the next step of TO or TH. Additionally, LSTM and GRU perform equivalently to RNN because operational parameters distant from the current cutterhead have negligible effects on future TBM performance.

We propose an innovative AC-RNN model, which integrates the historical operational parameters and the aware context of setting values. This model exhibits significant improvement in both cutterhead torque and thrust force forecasts. In sensitivity analysis, RPM_set plays an important role in both cutterhead torque and thrust force forecasts. Additionally, the last step cutterhead torque and thrust force themselves exert a significant influence on their respective future values.

Declaration of Generative AI and AI-assisted technologies in the writing process

During the preparation of this work the author(s) used ChatGPT in order to enhance the readability and logical flow of the language. After using this tool/service, the author(s) reviewed and edited the content as needed and take(s) full responsibility for the content of the publication.

CRediT authorship contribution statement

Feng Shan: Conceptualization, Data curation, Formal analysis, Investigation, Methodology, Software, Validation, Visualization, Writing – original draft. **Xuzhen He:** Investigation, Methodology, Validation, Writing – review & editing. **Danial Jahed Armaghani:** Formal analysis, Investigation, Writing – review & editing. **Haoding Xu:** Methodology, Software. **Xiaoli Liu:** Data curation, Resources. **Daichao Sheng:** Conceptualization, Project administration, Supervision, Writing – review & editing.

Declaration of competing interest

The authors declare that they have no known competing financial interests or personal relationships that could have appeared to influence the work reported in this paper.

Data availability

The authors do not have permission to share data.

References

Armaghani, D.J., Mohamad, E.T., Narayanasamy, M.S., Narita, N., Yagiz, S., 2017. Development of hybrid intelligent models for predicting TBM penetration rate in hard rock condition. Tunn. Undergr. Space Technol. 63, 29–43.
Barton, N., 1999. TBM performance estimation in rock using QTBM. T & T International 31 (9), 30–34.
Bergstra, J., Bengio, Y., 2012. Random search for hyper-parameter optimization. J. Mach. Learn. Res. 13 (2).
Bo, Y., Liu, Q., Huang, X., Pan, Y., 2022. Real-time hard-rock tunnel prediction model for rock mass classification using CatBoost integrated with Sequential Model-Based Optimization. Tunn. Undergr. Space Technol. 124, 104448.
Bruland, A., 1998. Hard rock tunnel boring. Norwegian University of Science and Technology, Trondheim, Norway.
Chen, Z., Liu, Y., Sun, H., 2021a. Physics-informed learning of governing equations from scarce data. Nat. Commun. 12 (1), 1–13.
Chen, R.-P., Zhang, P., Kang, X., Zhong, Z.-Q., Liu, Y., Wu, H.-N., 2019. Prediction of maximum surface settlement caused by earth pressure balance (EPB) shield tunneling with ANN methods. Soils Found. 59 (2), 284–295.
Chen, Z., Zhang, Y., Li, J., Li, X., Jing, L., 2021b. Diagnosing tunnel collapse sections based on TBM tunneling big data and deep learning: a case study on the Yinsong Project. China. *Tunnelling and Underground Space Technology* 108, 103700.
Cho, K., Van Merriënboer, B., Gulcehre, C., Bahdanau, D., Bougares, F., Schwenk, H. & Bengio, Y. (2014) Learning phrase representations using RNN encoder-decoder for statistical machine translation. *arXiv preprint arXiv:1406.1078*.
Erharter, G.H., Marcher, T., 2021. On the pointlessness of machine learning based time delayed prediction of TBM operational data. Autom. Constr. 121, 103443.
Feng, S., Chen, Z., Luo, H., Wang, S., Zhao, Y., Liu, L., Ling, D., Jing, L., 2021. Tunnel boring machines (TBM) performance prediction: A case study using big data and deep learning. Tunn. Undergr. Space Technol. 110, 103636.
Gao, X., Shi, M., Song, X., Zhang, C., Zhang, H., 2019. Recurrent neural networks for real-time prediction of TBM operating parameters. Autom. Constr. 98, 225–235.
Gao, M.-Y., Zhang, N., Shen, S.-L., Zhou, A., 2020. Real-time dynamic earth-pressure regulation model for shield tunneling by integrating GRU deep learning method with GA optimization. IEEE Access 8, 64310–64323.
Grima, M.A., Bruines, P., Verhoef, P., 2000. Modeling tunnel boring machine performance by neuro-fuzzy methods. Tunn. Undergr. Space Technol. 15 (3), 259–269.
Guo, D., Li, J., Jiang, S.-H., Li, X., Chen, Z., 2022. Intelligent assistant driving method for tunnel boring machine based on big data. Acta Geotech. 17 (4), 1019–1030.
Hasanpour, R., Rostami, J., Schmitt, J., Ozcelik, Y., Sohrabian, B., 2020. Prediction of TBM jamming risk in squeezing grounds using Bayesian and artificial neural networks. J. Rock Mech. Geotech. Eng. 12 (1), 21–31.
Hochreiter, S., 1998. The vanishing gradient problem during learning recurrent neural nets and problem solutions. Int. J. Uncertainty Fuzziness Knowledge Based Syst. 6 (02), 107–116.
Hochreiter, S., Schmidhuber, J., 1997. Long short-term memory. Neural Comput. 9 (8), 1735–1780.
Hou, S., Liu, Y., Yang, Q., 2022. Real-time prediction of rock mass classification based on TBM operation big data and stacking technique of ensemble learning. J. Rock Mech. Geotech. Eng. 14 (1), 123–143.
Jain, A.K., Mao, J., Mohiuddin, K.M., 1996. Artificial neural networks: A tutorial. Computer 29 (3), 31–44.

Karpatne, A., Atluri, G., Faghmous, J.H., Steinbach, M., Banerjee, A., Ganguly, A., Shekhar, S., Samatova, N., Kumar, V., 2017. Theory-guided data science: A new paradigm for scientific discovery from data. IEEE Trans. Knowl. Data Eng. 29 (10), 2318–2331.

Koopialipoor, M., Fahimifar, A., Ghaleini, E.N., Momenzadeh, M., Armaghani, D.J., 2020. Development of a new hybrid ANN for solving a geotechnical problem related to tunnel boring machine performance. Eng. Comput. 36, 345–357.

Li, J., Li, P., Guo, D., Li, X., Chen, Z., 2021. Advanced prediction of tunnel boring machine performance based on big data. Geosci. Front. 12 (1), 331–338.

Li, X., Wu, L.-J., Wang, Y., Liu, H., Chen, Z., Jing, L.-J., Wang, Y., 2023. A data driven real-time perception method of rock condition in TBM construction. *Can. Geotech. J.* **(ja)**.

Lin, Y., 1999. Study of BQ formula in national standard of quantitative classification for basic quality of rock mass. Chinese Journal of Geotechnical Engineering 21 (4), 481–485.

Liu, Z., Li, L., Fang, X., Qi, W., Shen, J., Zhou, H., Zhang, Y., 2021c. Hard-rock tunnel lithology prediction with TBM construction big data using a global-attention-mechanism-based LSTM network. Autom. Constr. 125, 103647.

Liu, M., Liao, S., Yang, Y., Men, Y., He, J., Huang, Y., 2021b. Tunnel boring machine vibration-based deep learning for the ground identification of working faces. J. Rock Mech. Geotech. Eng. 13 (6), 1340–1357.

Liu, B., Wang, Y., Zhao, G., Yang, B., Wang, R., Huang, D., Xiang, B., 2021a. Intelligent decision method for main control parameters of tunnel boring machine based on multi-objective optimization of excavation efficiency and cost. Tunn. Undergr. Space Technol. 116, 104054.

Mahdevari, S., Shahriar, K., Yagiz, S., Shirazi, M.A., 2014. A support vector regression model for predicting tunnel boring machine penetration rates. Int. J. Rock Mech. Min. Sci. 72, 214–229.

Ozdemir, L. (1977) Development of theoretical equations for predicting tunnel boreability.) Colorado School of Mines.

Qin, C., Shi, G., Tao, J., Yu, H., Jin, Y., Lei, J., Liu, C., 2021. Precise cutterhead torque prediction for shield tunneling machines using a novel hybrid deep neural network. Mech. Syst. Sig. Process. 151, 107386.

Qin, C., Shi, G., Tao, J., Yu, H., Jin, Y., Xiao, D., Zhang, Z., Liu, C., 2022. An adaptive hierarchical decomposition-based method for multi-step cutterhead torque forecast of shield machine. Mech. Syst. Sig. Process. 175, 109148.

Qin, C., Shi, G., Tao, J., Yu, H., Jin, Y., Xiao, D., Liu, C., 2024. RCLSTMNet: A Residual-convolutional-LSTM Neural Network for Forecasting Cutterhead Torque in Shield Machine. *Int. J. Control Autom. Syst.*:1–17.

Rostami, J., 1997. Development of a force estimation model for rock fragmentation with disc cutters through theoretical modeling and physical measurement of crushed zone pressure. Colorado School of Mines Golden.

Rostami, J., 2016. Performance prediction of hard rock Tunnel Boring Machines (TBMs) in difficult ground. Tunn. Undergr. Space Technol. 57, 173–182.

Rostami, J. & Ozdemir, L. (1993) A new model for performance prediction of hard rock TBMs. In *Proceedings of 1993 rapid excavation and tunneling conference.*), pp. 793-809.

Rostami, J., Ozdemir, L. & Nilson, B. (1996) Comparison between CSM and NTH hard rock TBM performance prediction models. In *Proceedings of Annual Technical Meeting of the Institute of Shaft Drilling Technology, Las Vegas.*), pp. 1-10.

Schuster, M., Paliwal, K.K., 1997. Bidirectional recurrent neural networks. IEEE Trans. Signal Process. 45 (11), 2673–2681.

Shan, F., He, X., Armaghani, D.J., Zhang, P., Sheng, D., 2022. Success and challenges in predicting TBM penetration rate using recurrent neural networks. Tunn. Undergr. Space Technol. 130, 104728.

Shan, F., He, X., Armaghani, D.J., Sheng, D., 2023a. Effects of data smoothing and recurrent neural network (RNN) algorithms for real-time forecasting of tunnel boring machine (TBM) performance. J. Rock Mech. Geotech. Eng.

Shan, F., He, X., Armaghani, D.J., Zhang, P., Sheng, D., 2023b. Response to Discussion on "Success and challenges in predicting TBM penetration rate using recurrent neural networks" by Georg H. Erharter, Thomas Marcher. Tunnelling and Underground Space Technology:105064.

Shan, F., He, X., Xu, H., Armaghani, D.J., Sheng, D., 2023c. Applications of Machine Learning in Mechanised Tunnel Construction: A Systematic Review. Eng 4 (2), 1516–1535.

Shen, S.-L., Yan, T., Zhou, A., 2023. Estimating locations of soil–rock interfaces based on vibration data during shield tunnelling. Autom. Constr. 150, 104813.

Shi, G., Qin, C., Tao, J., Liu, C., 2021. A VMD-EWT-LSTM-based multi-step prediction approach for shield tunneling machine cutterhead torque. Knowl.-Based Syst. 228, 107213.

Sobol, I.M., 1990. On sensitivity estimation for nonlinear mathematical models. Matematicheskoe Modelirovanie 2 (1), 112–118.

Sousa, R.L., Einstein, H.H., 2012. Risk analysis during tunnel construction using Bayesian Networks: Porto Metro case study. Tunn. Undergr. Space Technol. 27 (1), 86–100.

Srivastava, N., Hinton, G., Krizhevsky, A., Sutskever, I., Salakhutdinov, R., 2014. Dropout: a simple way to prevent neural networks from overfitting. The Journal of Machine Learning Research 15 (1), 1929–1958.

Suwansawat, S., Einstein, H.H., 2006. Artificial neural networks for predicting the maximum surface settlement caused by EPB shield tunneling. Tunn. Undergr. Space Technol. 21 (2), 133–150.

Wang, R., Li, D., Chen, E.J., Liu, Y., 2021a. Dynamic prediction of mechanized shield tunneling performance. Autom. Constr. 132, 103958.

Wang, X., Zhu, H., Zhu, M., Zhang, L., Ju, J.W., 2021b. An integrated parameter prediction framework for intelligent TBM excavation in hard rock. Tunn. Undergr. Space Technol. 118, 104196.

Wu, A., Zhao, W., Zhang, Y., Fu, X., 2023. A detailed study of the CHN-BQ rock mass classification method and its correlations with RMR and Q system and Hoek-Brown criterion. Int. J. Rock Mech. Min. Sci. 162, 105290.

Xiao, H.-H., Yang, W.-K., Hu, J., Zhang, Y.-P., Jing, L.-J., Chen, Z.-Y., 2022. Significance and methodology: Preprocessing the big data for machine learning on TBM performance. Underground Space 7 (4), 680–701.

Xu, C., Liu, X., Wang, E., Wang, S., 2021. Prediction of tunnel boring machine operating parameters using various machine learning algorithms. Tunn. Undergr. Space Technol. 109, 103699.

Yagiz, S., 2008. Utilizing rock mass properties for predicting TBM performance in hard rock condition. Tunn. Undergr. Space Technol. 23 (3), 326–339.

Yagiz, S. (2002) Development of rock fracture and brittleness indices to quantify the effects of rock mass features and toughness in the CSM model basic penetration for hard rock tunneling machines.

Yang, J., Yagiz, S., Liu, Y.-J., Laouafa, F., 2022. Comprehensive evaluation of machine learning algorithms applied to TBM performance prediction. Underground Space 7 (1), 37–49.

Zhang, Q., Liu, Z., Tan, J., 2019. Prediction of geological conditions for a tunnel boring machine using big operational data. Autom. Constr. 100, 73–83.

Zhang, P., Wu, H.-N., Chen, R.-P., Chan, T.H., 2020. Hybrid meta-heuristic and machine learning algorithms for tunneling-induced settlement prediction: A comparative study. Tunn. Undergr. Space Technol. 99, 103383.

Zhou, J., Qiu, Y., Armaghani, D.J., Zhang, W., Li, C., Zhu, S., Tarinejad, R., 2021. Predicting TBM penetration rate in hard rock condition: a comparative study among six XGB-based metaheuristic techniques. Geosci. Front. 12 (3), 101091.